A Digital Quantum Algorithm for Non-Markovian Electron Transfer Dynamics Using Repeated Interactions

Lea K. Northcote, $^{1,*)}$ Matthew S. Teynor, $^{1,2,*)}$ and Gemma C. Solomon $^{1,2,\dagger)}$

(Dated: 25 February 2025)

Quantum algorithms have the potential to revolutionize our understanding of open quantum systems in chemistry. In this work, we demonstrate that quantum algorithms leveraging a repeated interaction model can effectively reproduce non-Markovian electron transfer processes under four different donor-acceptor parameter regimes and for a donor-bridge-acceptor system. We systematically explore how the algorithm scales for the regimes. Notably, our approach exhibits favorable scaling in the required repeated interaction length as the electronic coupling, temperature, damping rate, and system size increase. Furthermore, a single Trotter step per repeated interaction leads to an acceptably small error, and high-fidelity initial states can be prepared with a short time evolution. This efficiency highlights the potential of the algorithm for tackling increasingly complex systems. When fault-tolerant quantum hardware becomes available, the method could be extended to incorporate structured baths, additional energy levels, or more intricate coupling schemes, enabling the simulation of real-world open quantum systems that remain beyond the reach of classical computation.

I. INTRODUCTION

Quantum algorithm research for chemistry has often concentrated on calculating static properties for complex electronic structure problems; however, simulations of chemical dynamics, especially open system dynamics, would also benefit from a level of accuracy that classical computation may not be able to achieve. 1,2 Open quantum systems interact with the environment and the resulting decoherence and relaxation can be challenging to capture fully with classical computation. This challenge becomes even larger for systems that strongly couple to the environment and have non-Markovian effects.^{3,4} For classical simulations of open quantum systems, storing the density matrix usually requires memory that scales exponentially with the size of the system, which limits the systems that can be studied and the methods that can be applied. Because quantum computers encode information in qubits, we can circumvent the exponential scaling issues encountered when encoding quantum states with classical bits.⁵

Analog quantum simulators are a promising avenue for modeling chemically relevant open quantum systems. For an analog simulation, a quantum device is engineered so that the non-unitary dynamics of a chemical system can be mapped directly onto the dynamics of the device. Studies have proposed strategies for performing analog simulations of molecular open quantum systems on superconducting,^{6,7} trapped ion,^{8–10} semiconductor quantum dot,¹¹ and photonic¹² quantum devices. With the improved quality of quantum hardware, we have be-

gun to see experimental realizations of these analog simulations. So et al. simulated charge transfer dynamics across multiple parameter regimes on a trapped ion device. 13 Sun et al. implemented a method for structured baths on trapped ion hardware to simulate vibrationassisted energy transfer. 4 Also on a trapped ion device, Navickas et al. recently performed open-system molecular dynamics simulations of photoexcited pyrazine. ¹⁵. In addition to these trapped ion results, there have been experimental realizations using photonics¹⁶ and nuclear magnetic resonance¹⁷. While these approaches are promising, analog quantum computation is fundamentally constrained to certain parameter regimes dictated by the physics of the underlying device. In contrast, digital quantum algorithms can reach arbitrary parameter regimes, under the assumption that there will be faulttolerant hardware with large numbers of qubits that can reach large circuit depths. Therefore, while analog simulations may provide new insights into certain open quantum systems, digital approaches promise broader applicability in the future fault-tolerant quantum computing era.

It is not straightforward to encode the non-unitary dynamics of open quantum systems in a digital quantum algorithm because the building blocks of digital quantum computing, quantum gates, are unitary. A general strategy to overcome this challenge is to introduce ancilla qubits and embed non-unitary operators within higher-dimensional unitary gates. Various methods building on this strategy have been developed, including dilation or block-encoding methods, ^{18–25} quantum imaginary time evolution (QITE), ²⁶ variational approaches, ^{27–41} and tensor train approaches. ⁴² Notably, dilation methods based on singular value decomposition (SVD) have shown significant promise for simulating chemically relevant dynamics on near-term quantum hardware. For

¹⁾ NNF Quantum Computing Programme, Niels Bohr Institute, University of Copenhagen, DK-2100 Copenhagen Ø, Denmark

 $^{^{2)}}$ Nano-Science Center and Department of Chemistry, University of Copenhagen, DK-2100 Copenhagen \emptyset , Denmark

^{*)}Contributed equally

^{†)}Email: gsolomon@chem.ku.dk

instance, Hu et al. applied SVD techniques to simulate Lindblad dynamics of the Fenna-Matthews-Olson (FMO) complex, a photosynthetic antenna that channels excitation energy to the reaction center in photosynthesis. ⁴³ Dan et al. also used SVD to implement a quantum algorithm based on the hierarchical equations of motion to model the non-Markovian dynamics of FMO and charge and energy transport in molecular systems. ⁴⁴ These studies are promising, but SVD methods require diagonalization of the propagator, which may limit how the method can be applied in the future.

Recently, quantum algorithms that rely on repeated interaction models have demonstrated considerable potential. 45-47 These methods use mid-circuit measurements on ancilla qubits to introduce non-unitary effects, see Figure 1. In this framework, the system of interest is coupled to an ancilla qubit register, and the combined system repeatedly undergoes a short unitary evolution before the ancilla is measured and reset to an initial state. The joint unitary evolution and the initial state of the ancilla can be designed to reproduce both Markovian and non-Markovian dynamics of the system of interest.⁴⁸ Pocrnic et al. gave an analytic proof that quantum circuits based on repeated interaction models can replicate Lindblad dynamics to a given error, where the upper bound for the required number of mid-circuit measurements is inversely proportional to the error, meaning that smaller errors can be achieved by increasing the rate of mid-circuit measurements. 45 Gallina et al. used a repeated interaction scheme to simulate energy transfer in a two-chromophore system, focusing on how to calculate response functions with a quantum algorithm.⁴⁷ While these advancements are promising, the practical utility of simulating chemical systems with repeated interactions remains underexplored. Specifically, previous studies have either focused on proving worst-case scenario error bounds or applying the method to a specific system, leaving a gap in understanding how these algorithms scale for different chemical regimes.

Electron transfer (ET) reactions offer an ideal test case for investigating how the repeated interaction method scales for chemical systems. ET reactions involve the transfer of an electron from a donor to an acceptor and are fundamental across chemistry, from photosynthesis to catalysis. Compared to other model systems, such as energy transfer, ET reactions typically have stronger coupling between the electronic and nuclear degrees of freedom. This strong vibronic coupling arises from a significant reorganization of the nuclear coordinates as the electronic state changes. Due to this strong coupling, ET dynamics can exhibit non-Markovian effects, where the nuclear degrees of freedom do not act as a memoryless bath. To account for this, foundational models for ET reactions explicitly treat both the electronic system and a collective reaction coordinate.⁴⁹ The reaction coordinate can interact with the environment, making reactions irreversible and necessitating an open quantum system treatment. ET reactions are appealing for test-

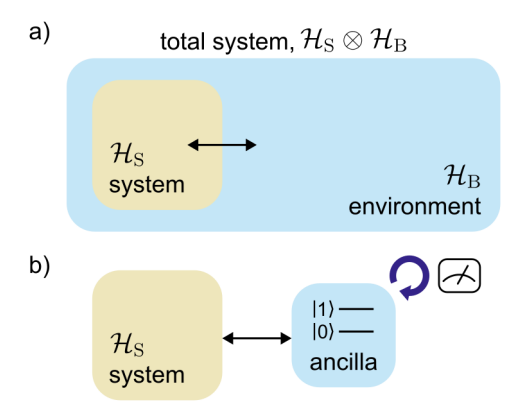


FIG. 1. Open Quantum Systems and the Repeated Interaction Model. (a) Illustration of an open quantum system. The system resides in the Hilbert space \mathcal{H}_S and interacts with the surrounding environment described by \mathcal{H}_B to give the total system that exists in the combined Hilbert space. (b) Schematic of the repeated interaction model. The effect of the environment on the system is captured by having the system interact with an ancilla qubit that is repeatedly reset with mid-circuit measurements. The ancilla qubit and the measurements allow for the simulation of non-unitary system dynamics.

ing quantum algorithms because the dynamics are complicated, but well-understood, for basic models. So even though we are unlikely to learn new chemistry by simulating simple ET models, these models give us a measure to evaluate when quantum algorithms will give chemically meaningful results. Additionally, relevant ET reactions span many parameter regimes, ⁵⁰ which allows for systematic testing of algorithmic scaling across a large parameter range. For these reasons, we chose to investigate how repeated interaction algorithms scale for ET reactions.

In this paper, we aim to connect theoretical error bounds and practical applicability by examining the scaling behavior of a quantum algorithm using repeated interactions for ET reaction dynamics. Specifically, we focus on donor-acceptor (DA) systems to investigate how this algorithm performs as the electronic coupling, the temperature, and the damping rate increase. Furthermore, we extend the model to a donor-bridge-acceptor (DBA) system to investigate the effect of increasing the system size. We evaluate the performance of the algorithm, specifically focusing on how often the mid-circuit measurements must be performed to recover the correct dynamics. In addition, we validate the algorithm by ensuring that generating initial states and factoring the overall dynamics into easily implementable, sequential operations through Trotter formulas is feasible. Our numerical simulations provide insight into the practical capabilities of quantum algorithms based on the repeated interaction model.

In Section 2, we outline the concepts from ET theory, which we use to construct our system Hamiltonian, as well as the Lindblad master equation used for the open quantum system description. We move on to describe the quantum algorithm concepts used in this paper including repeated interaction schemes, Trotter formulas, and state preparation. We then present the details of our numerical simulations in Section 3 and our results in Section 4. Finally, we provide a discussion of our results in Section 5 which ends with a summary of our main conclusions.

II. THEORY

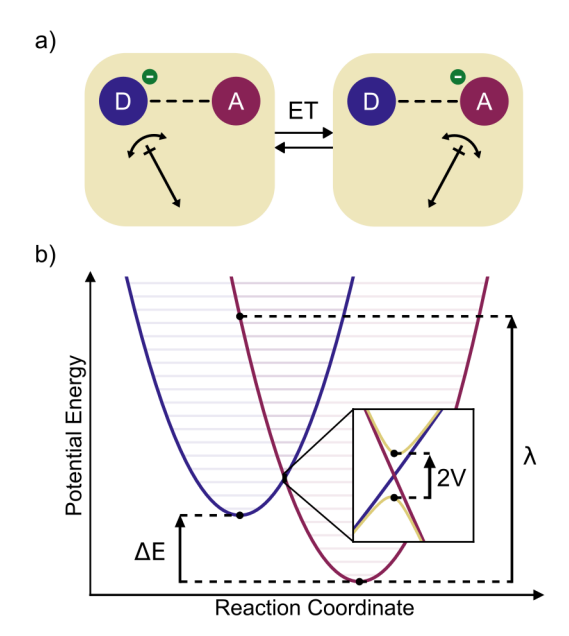
A. Electron transfer dynamics

For ET reactions, the key simulation target is the transfer rate of the electron moving from the donor to the acceptor. To simulate the transfer dynamics, rather than treating all the interactions between the electron and the nuclear degrees of freedom in the environment, we model the electron as interacting with a collective degree of freedom, called the reaction coordinate, which then interacts with the broader environment. The compression of the nuclear degrees of freedom can be visualized as replacing the nuclei with a single dipole that rotates to align with the electron, where the angle of the dipole is the reaction coordinate, as depicted in Figure 2a. Our strategy for obtaining the transfer rate is to write a model Hamiltonian that extends the electronic system to a supersystem that includes a reaction coordinate. This has been shown to capture non-Markovian effects for systems with strong system-bath coupling and for structured environments.⁵¹ We then use the Lindblad formalism to describe the interaction between the reaction coordinate and the environment, using jump operators to govern these interactions. These jump operators form the basis of the repeated interaction algorithm, which we use to simulate the open system dynamics over time.

The supersystem model for a donor-acceptor ET system has a main electronic system and a reaction coordinate. The electronic system is a two-level system with diabatic states $|D\rangle$ and $|A\rangle$ that represents the electron localized on either the donor or acceptor. We model the reaction coordinate as a single harmonic oscillator, where the equilibrium energy and position depend on the electron. The donor-acceptor Hamiltonian can be written using creation and annihilation operators \hat{a}^{\dagger} and \hat{a} for the reaction coordinate and Pauli matrix notation for the electronic system (i.e., $\sigma^{(z)} = |D\rangle\langle D| - |A\rangle\langle A|$ and $\sigma^{(x)} = |D\rangle\langle A| + |A\rangle\langle D|$) as

$$H_{\rm DA} = \frac{1}{2} \Delta E \sigma^{(z)} + V \sigma^{(x)} + \hbar \omega \hat{a}^{\dagger} \hat{a} + \sqrt{\hbar \omega \lambda} \sigma^{(z)} \hat{q}. \quad (1)$$

The first term in this Hamiltonian gives the energy separation, ΔE , between the donor and acceptor states, following the sign convention that ΔE is the donor energy minus the acceptor energy. The second term in the Hamiltonian is the electronic coupling, V, between the



Reaction Coordinate Model for Electron **Transfer.** (a) Schematic representation of the reaction coordinate responding to the transferring electron. The nuclear degrees of freedom are approximated as a single dipole that aligns with the localization of the electron. In this picture, the angle of the dipole is the reaction coordinate. The dipole will rotate slightly around the equilibrium position due to thermal fluctuations. (b) Diabatic potential energy surfaces for the donor (blue) and acceptor (red) states as a function of the reaction coordinate. The inset shows the avoided crossing, with the adiabatic surfaces as yellow lines. Horizontal lines in the parabolas indicate quantized vibrational energy levels for each surface. Arrows show the donor-acceptor energy gap ΔE , the reorganization energy λ , and two times the electronic coupling 2V. Together, these visualizations illustrate how the reaction coordinate mediates electron transfer and how key energetic parameters shape the transfer dynam-

donor and acceptor states. The third term is the reaction coordinate harmonic oscillator with frequency ω . The last term gives the coupling between the electron and the reaction coordinate. This coupling is between $\sigma^{(z)}$ for the electron and the position of the harmonic oscillator, $\hat{q} = (\hat{a}^{\dagger} + \hat{a})/2$, so it can be understood as shifting the potential energy minimum of the harmonic oscillator by $-\sqrt{\lambda/(\hbar\omega)/2}$ for the donor state and by $+\sqrt{\lambda/(\hbar\omega)/2}$ for the acceptor state. These shifts, along with the donoracceptor energy gap, give rise to the two parabolas in the diabatic potential energy surface shown in Figure 2b. The strength of this coupling is quantified by the reorganization energy, λ . The reorganization energy is the energy that would be released as the reaction coordinate goes from the minimum energy position of the acceptor state to the minimum energy position of the donor state while the electron is at the acceptor state. The adiabatic potential energy surface, which includes the effect of the electronic coupling, V, has an avoided crossing as shown

in the inset of Figure 2b.

The parameters in the Hamiltonian can take on a large range of chemically relevant values. When the electronic coupling, V, is small compared to the other energy scales, the reaction falls within the nonadiabatic regime. ⁵⁰ For nonadiabatic ET reactions, if the thermal energy is large relative to the oscillator energy $(k_{\rm B}T\gg\hbar\omega)$, the rate of the reaction can be predicted with Marcus theory. Alternatively, if the thermal energy is comparable to or smaller than the oscillator energy, the reaction rate can be modeled with Fermi's golden rule. In the adiabatic regime, when the electronic coupling is comparable to other energy scales, the reaction rate cannot be modeled by Fermi's golden rule or Marcus theory.

The DA model can be expanded to include bridging units, modeled as other diabatic states between the donor and acceptor. For the DBA system, the bridge states are labeled as $|B_i\rangle$ for the *i*th bridge unit from the donor. In this study, we included two bridging units in our version of the DBA model because the four total sites can be naturally encoded into two qubits. The Hamiltonian for a DBA system with two bridging units can be written as

$$H_{\text{DBA}} = \sum_{\phi} \left(\epsilon_{\phi} + \hbar \omega \left(\hat{q} - q_{\phi} \right)^{2} \right) |\phi\rangle \langle \phi| + \hbar \omega \hat{p}^{2}$$
$$+ V \left(|D\rangle \langle B_{1}| + |B_{1}\rangle \langle B_{2}| + |B_{2}\rangle \langle A| + \text{h.c.} \right), (2)$$

where the sum goes over $\phi = \{D, B_1, B_2, A\}$ and h.c. stands for Hermitian conjugate. The energy and equilibrium position of the reaction coordinate are given by ϵ_{ϕ} and q_{ϕ} for each of the electronic diabatic states. This model assumes equal coupling between neighboring units and no long-range coupling between next-nearest neighbors or directly between the donor and acceptor. We have also introduced the momentum of the reaction coordinate, $\hat{p} = i \left(\hat{a}^{\dagger} - \hat{a} \right) / 2$. The Hamiltonian gives a diabatic potential energy surface that has four parabolas along the reaction coordinate, rather than the two for the DA model.

The unitary dynamics generated by the DA Hamiltonian (Equation 1) and the DBA Hamiltonian (Equation 2) do not fully describe the reaction dynamics. Augmenting the electronic system with the reaction coordinate is only the first step in accounting for the effect of the nuclear degrees of freedom, and we must also consider the relaxation of the reaction coordinate. We use the Lindblad equation,

$$\frac{\partial \rho}{\partial t} = \mathcal{L}\rho = -\frac{i}{\hbar} \left[H_{\rm ET}, \rho \right] + \mathcal{D} \left(\rho \right), \tag{3}$$

where $H_{\rm ET}$ could be either $H_{\rm DA}$ or $H_{\rm DBA}$, to describe the time dependence of the density matrix of the supersystem, ρ . The dissipator, $\mathcal{D}(\rho)$, has the form of a standard dissipator for the damped harmonic oscillator,

$$\mathcal{D}(\rho) = \gamma \left(1 + \bar{n}\right) \left(L\rho L^{\dagger} - \frac{1}{2} \left\{L^{\dagger} L, \rho\right\}\right) + \gamma \bar{n} \left(L^{\dagger} \rho L - \frac{1}{2} \left\{L L^{\dagger}, \rho\right\}\right), \tag{4}$$

with a decay rate of γ and an average harmonic oscillator mode population given by a Boltzmann distribution, $\bar{n} = (\exp(\hbar\omega/(k_{\rm B}T))-1)^{-1}$, and where $\{A,B\}$ is the anticommutator given by $AB+BA.^{52}$ The jump operators L and L^{\dagger} are shifted to account for the shift in the minimum energy position induced by the coupling between the electron and the reaction coordinate:

$$L = \hat{a} - \delta_{\rm ET},\tag{5}$$

with the shift for the DA system given by

$$\delta_{\rm DA} = -\frac{1}{2} \sqrt{\frac{\lambda}{\hbar \omega}} \sigma^{(z)},\tag{6}$$

and the shift for the DBA system given by

$$\delta_{\rm DBA} = \sum_{\phi} q_{\phi} |\phi\rangle\langle\phi|. \tag{7}$$

A similar shift of the Lindblad jump operators was used recently to model proton transfer. 53

We use the Lindblad equation to model the Markovian dynamics of the supersystem, which can result in non-Markovian dynamics for the electronic system. The Lindblad equation relies on the separability of the initial state between the bath and system, and the Born-Markov and secular approximations.⁵² These assumptions are justified if there is weak coupling between the system and the bath. For modeling the ET supersystem dynamics with the Lindblad equation, we only assume that there is weak coupling between the reaction coordinate and the broader environment. We do not consider the case where the broader environment directly interacts with the electronic system. The Markovian dynamics of a reaction coordinate supersystem has been shown to preserve the non-Markovian dynamics of the main system for problems with a similar structure.⁵¹ We can confirm the non-Markovian nature of the main system dynamics by quantifying the information backflow from the reaction coordinate into the system, which can show that the reaction coordinate does not act as a memoryless bath.⁵⁴

B. Non-unitary dynamics on a unitary quantum computer

Simulating non-unitary dynamics on a unitary quantum computer presents distinct challenges. To perform a digital quantum simulation of an ET reaction, the non-unitary dynamics described by the Lindblad equation (Equation 3) must be encoded in the operations available to a digital quantum computer—namely, unitary gates and measurement. In this study, we use a repeated interaction scheme, sometimes called a quantum collision model, to simulate non-unitary ET dynamics. The main idea of this scheme is to repeatedly perform a unitary evolution on the system of interest coupled to an ancilla system and then measure and reset the ancilla for each short time step. Figure 3 shows a quantum circuit

diagram for this general scheme. Repeated interaction models are often studied in contexts where the discrete dynamics arise naturally, such as a system that occasionally collides with another system. However, this is not the case in this study. We are using a repeated interaction model because it can approximate Lindblad dynamics, even though repeated interactions do not obviously arise in ET theory.

$$\rho(t_0) = \left(\frac{1}{\eta_a} - \frac{U(\tau)}{U(\tau)} \right)^{\times t/\tau} \approx e^{\mathcal{L}t} \rho(t_0)$$

FIG. 3. General Quantum Circuit for the Repeated Interaction Model. The first qubit register (top line) represents the system of interest, while the second qubit register (bottom line) represents the ancilla. $\rho(t_0)$ is the initial state of the system of interest and η_a is the initial state of the ancilla qubit register. The system and ancilla have a joint unitary operation $U(\tau)$ that evolves the combined system for a short time τ . The ancilla is then measured and reset to its initial state. The process in brackets is repeated t/τ times, allowing the circuit to approximate the Lindblad evolution of the system of interest over a total time t. This iterative approach enables the simulation of open quantum system dynamics within a fault-tolerant quantum computing framework.

We can precisely define the repeated interaction model as repeatedly applying a dynamical map to the system. The state of a system after s interactions each of length τ is represented mathematically by

$$\rho(t_0 + s\tau) = \mathcal{E}_s \left[\dots \mathcal{E}_2 \left[\mathcal{E}_1 \left[\rho(t_0) \right] \right] \right]$$

= $\mathcal{E}^s \left[\rho(t_0) \right],$ (8)

where t_0 is the initial time. The dynamical map,

$$\mathcal{E}\left[\rho\right] = \operatorname{Tr}_{a}\left\{U(\tau)\left(\rho \otimes \eta_{a}\right) U^{\dagger}(\tau)\right\},\tag{9}$$

describes how the system and the ancilla in some initial state η_a undergo joint unitary evolution defined by U, before the ancilla system is traced out.

Following the work of Pocrnic et al., 45 the joint unitary for the system-ancilla evolution is

$$U(\tau) = \exp\left\{-\frac{i\tau}{\hbar} \left(H_{\rm ET} + \frac{1}{\sqrt{\tau}} H_{\rm int}\right)\right\}, \quad (10)$$

where $H_{\rm ET}$ is either $H_{\rm DA}$ or $H_{\rm DBA}$. The factor of $1/\sqrt{\tau}$ is a standard feature of repeated interaction models that creates a diverging coupling strength to the ancilla and preserves the dynamics in the limit of τ approaching zero. ⁴⁸ In general, the ancilla system could also have internal dynamics described by operators that only act on the ancilla system; however, this is not needed to reproduce Lindblad dynamics. The Hamiltonian describing the interaction between the system and the ancilla is

$$H_{\rm int} = \sqrt{\gamma (2\bar{n} + 1)} \left(L \otimes \sigma_a^{(+)} + L^{\dagger} \otimes \sigma_a^{(-)} \right), \quad (11)$$

where L and L^{\dagger} are the jump operators defined by Equation 5, and $\sigma_a^{(+)} = |1\rangle_a \langle 0|$ and $\sigma_a^{(-)} = |0\rangle_a \langle 1|$ are the two-level system creation and annihilation operators, with the subscript a denoting that they act on the ancilla qubit. The ancilla initial state is

$$\eta_a = \frac{1}{2\bar{n} + 1} (\bar{n} |0\rangle_a \langle 0| + (\bar{n} + 1) |1\rangle_a \langle 1|).$$
(12)

To simulate an ET process, the dynamics start with an initial state of the supersystem, $\rho(t_0)$, which has the electronic system localized on the donor and the reaction coordinate equilibrated relative to the localized electron. This is described by

$$\rho(t_0) = |D\rangle\langle D| \frac{e^{-\beta\langle D|H_{\rm ET}|D\rangle}}{Z}, \tag{13}$$

with $\beta=1/(k_{\rm B}T)$ and a normalization constant $Z={\rm Tr}\left\{e^{-\beta\langle D|H_{\rm ET}|D\rangle}\right\}$, where $H_{\rm ET}$ is either $H_{\rm DA}$ or $H_{\rm DBA}$. The exponential gives the equilibrated state of the reaction coordinate, which is a thermal harmonic oscillator state that has been displaced to the potential energy minimum position of the donor state.

The displaced thermal state for the reaction coordinate can be prepared on a quantum computer using the same repeated interaction scheme that generates the dynamics of interest. The state preparation begins with the electron in the donor state and the reaction coordinate in an easy-to-prepare state, such as the ground state. A modification of the repeated interaction unitary (Equation 10) can be used to transform the easy-to-prepare state into the displaced thermal state when evolved for a long enough time. The state preparation procedure should not allow the electron to transfer from the donor, so electronic coupling to the donor should not be included. The state preparation (SP) unitary is then

$$U_{\rm SP}(\tau) = \exp\left\{-\frac{i\tau}{\hbar} \left(H_{\rm ET}^{(0)} + \frac{1}{\sqrt{\tau}} H_{\rm int}\right)\right\},\tag{14}$$

where $H_{\rm ET}^{(0)}$ is either $H_{\rm DA} - V \sigma^{(x)}$ or $H_{\rm DBA} - V (|D\rangle\langle B_1| + |B_1\rangle\langle D|)$. In our numerical simulations, we monitored the progress of this state preparation procedure using the fidelity, defined as

$$F(\rho, \sigma) = \text{Tr}\left\{\sqrt{\rho^{1/2}\sigma\rho^{1/2}}\right\},\tag{15}$$

between the time-evolved state and the exact initial state defined in Equation 13.

The repeated interaction unitary (Equation 10) cannot be implemented directly during a digital quantum simulation because the exponential contains terms that would need to act on the same qubits simultaneously. We therefore use a Trotter formula to split the unitary into factors that can each be implemented sequentially for a small time step.⁵ Implementing these factors one at a time introduces an error when the factors do not commute. This error can be suppressed by using higher-order Trotter formulas or decreasing the length of the

time step. For the repeated interaction scheme, the total time needed for the dynamics, t, is already split into steps of length τ . With the Trotter formula, each τ step will be further factored into n Trotter steps. Given some value of τ needed to reproduce Lindblad dynamics, the goal for implementing the Trotter formula is to optimize the number of Trotter steps per τ by balancing accuracy with the number of operations.

To numerically investigate this trade-off between accuracy and the number of operations for the donor-acceptor ET simulations, we use a 2nd-order Trotter formula, 55

$$U(\tau) \approx U_{\text{Trotter}}(\tau) = \left(\prod_{k=1}^{6} \exp\left\{-\frac{i}{\hbar} \frac{\tau}{2n} H_k\right\} \prod_{k=6}^{1} \exp\left\{-\frac{i}{\hbar} \frac{\tau}{2n} H_k\right\}\right)^{n}. \quad (16)$$

The six H_k factors come from the four terms in H_{DA} and the two terms in $H_{\mathrm{int}}/\sqrt{\tau}$. These six factors are sorted in descending order so the k=1 factor has the largest coefficient. The second product in this Trotter formula reapplies the H_k factors in the opposite order, which is the key difference between 1st- and 2nd-order Trotter formulas. In a hardware-specific implementation, the six factors might be further divided based on which specific gates are available, and how the operators are encoded, but this is not considered in this study.

III. NUMERICAL SIMULATION DETAILS

To study how a repeated interaction scheme can be used in a quantum algorithm to model ET, we performed numerical simulations using the four parameter sets listed in Table I. We chose these parameter sets to systematically evaluate how the repeated interaction algorithm scales while ensuring the numerical simulations were feasible, rather than attempting to model specific systems. This means that the parameter sets do not unambiguously fall into single, well-defined chemical regimes, such as nonadiabatic vs. adiabatic. The first parameter set, which we label as weakly coupled because of the small electronic coupling, V, serves as the reference for the other three sets. The strongly damped parameter set increases the damping rate, γ , of the reaction coordinate, representing a system with stronger dissipation. The strongly coupled parameter set features a larger electronic coupling while keeping all other parameters identical to the weakly coupled parameter set. Finally, the high-temperature parameter set increases the thermal energy, $k_{\rm B}T$, along with the accompanying higher reorganization energy, λ , reflecting conditions where classical transfer effects become more prominent. The three parameter sets with $k_{\rm B}T=1$ are collectively labeled as low temperature.

In addition to the four DA parameter sets, we also investigated a DBA system. This system was configured with the same electronic coupling, thermal energy, and damping rate as the weakly coupled parameter set. The

spacing between all neighboring units was set to $\hat{q}=1$, matching the DA distance in the weakly coupled case. Relative to the acceptor energy, the site energies of the donor and bridge units were chosen as $\epsilon_D=5\hbar\omega$, $\epsilon_{B_1}=4\hbar\omega$, and $\epsilon_{B_2}=3\hbar\omega$.

We truncated the Hilbert space of the reaction coordinate in our numerical simulations, which would also be required for the simulation of a harmonic oscillator on a digital quantum computer. For the low-temperature parameter sets, the reaction coordinate was truncated to 16 energy levels, corresponding to a four-qubit binary encoding, while for the high-temperature parameter set, it was truncated to 32 energy levels, requiring five qubits. We ensured the truncation did not appreciably affect the dynamics by inspecting the expectation value of the initial position for the harmonic oscillator (see Figure S1 in the Supplementary Material) and the transfer rate error from Lindblad simulations for different numbers of qubits (Figures S2–S3). It is interesting to note that rather than thermal energy, the primary factor determining the necessary truncation was the displacement of the minimum energy positions, given by $\pm \sqrt{\lambda/(\hbar\omega)/2}$ for the DA systems. This is because displaced oscillator states require a large number of basis states to be accurately represented in the original oscillator basis, even when thermal energy is relatively small.

We confirmed that the parameter regimes display non-Markovian dynamics by measuring the information backflow from the reaction coordinate to the electron. We observed information backflow for Lindblad simulations for all the low-temperature donor-acceptor parameter sets, but not for the high-temperature set. We also confirmed that the repeated interaction model preserves the same information backflow. See Supplementary Material Section II for a detailed description of these calculations and results.

We used QuTiP version 5.0.2 to perform the numerical integration of the Lindblad master equation and the repeated interaction scheme. Each simulation was run over a time interval from t=0 to $t=1000(2\pi/\omega)$. To calculate the transfer rate k, the donor population was fit using SciPy version 1.13.1 to an exponential decay of the form $P_D(t) = P_D(0) \exp\{-kt\}$ where P_D is the donor population.

IV. RESULTS

We show the donor populations as a function of time in Figure 4 from repeated interaction simulations (numerical evaluations of Equation 8) for the four DA parameter sets—weakly coupled, strongly damped, strongly coupled, and high temperature—with values of the energy gap, ΔE , that led to fast transfer. The repeated interaction model successfully reproduced the Lindblad dynamics (numerical evaluations of Equation 3) using an interaction length of $\tau = 0.1(2\pi/\omega)$ for the low-temperature parameter sets and $0.01(2\pi/\omega)$ for the high-temperature

TABLE I. Simulation Parameters for Donor-Acceptor Electron Transfer. The weakly coupled parameter set serves as the reference for the other three parameter sets. Each of the remaining sets varies a single parameter to explore different electron transfer regimes, except for the high-temperature set, where both the thermal energy and the reorganization energy are increased due to their inherent dependence on each other.

Parameter set	Electronic	Reorganization	Thermal	Damping
	coupling,	energy,	energy,	rate,
	$V\left(\hbar\omega\right)$	$\lambda \left(\hbar \omega \right)$	$k_{\mathrm{B}}T\left(\hbar\omega\right)$	$\gamma \left(\omega /2\pi \right)$
Weakly coupled	0.1	1	1	0.01
Strongly damped	0.1	1	1	$1/(2\pi) \approx 0.16$
Strongly coupled	1	1	1	0.01
High temperature	0.1	20	2	0.1

parameter set. We saw coherent oscillations in the donor population from the Lindblad and converged repeated interaction simulations. In general, when the repeated interaction length was too large, we saw too many oscillations, resembling unitary dynamics.

In Figure 5, we show the donor population from repeated interaction simulations with different interaction lengths, along with the population dynamics of each site of the DBA model. Similar to the low-temperature DA parameter sets, the DBA simulation converged to the Lindblad result with an interaction length of 0.1 $(2\pi/\omega)$. The DBA model exhibited a quicker transfer from the donor state compared to the DA simulations, suggesting that the inclusion of bridges provides either an effectively stronger coupling or more favorable dynamics. The DBA system exhibited hopping behavior, characterized by the sequential transfer of population between localized states as seen in Figure 5b. Initially, the population resided on the donor, which then transferred to the first bridge site, followed by the second bridge site, and then ultimately to the acceptor. This stepwise transfer reflects the intermediate role of the bridge sites in facilitating the ET process. The dynamics of hopping are influenced by the coupling strengths between adjacent sites, as well as the interaction with the environment, which can introduce decoherence or dissipation. Furthermore, coherent oscillations were observed between the states, which were evident in all low-temperature parameter sets explored in this study. In more classical or strongly damped conditions, the transfer should appear smoother and less oscillatory.

The transfer dynamics simulated with the repeated interaction model also converged across values for the donor-acceptor energy gap ΔE to the Lindblad results for the low-temperature DA systems with a repeated interaction length of $0.1(2\pi/\omega)$. In Figure 6, the transfer rates obtained from repeated interaction simulations with different values of τ are plotted against the DA energy gap. Figure 6a shows the transfer rates for the weakly coupled parameters, where narrow peaks are seen on resonance with integer multiples of $\hbar\omega$. Figure 6b is the transfer rates for the strongly damped parameter set, where as expected the peaks are broader than the peaks from the weakly coupled parameter set. Figure 6c shows the rates for the strongly coupled parameter set. With these

parameters, we see peaks that are even broader and no longer on resonance with $\hbar\omega$. For both the weakly coupled and the strongly coupled parameters, using too large of an interaction length led to peaks at the same value of ΔE but with a smaller transfer rate than the Lindblad results. Interestingly for the strongly damped case, using too large of an interaction length led to peaks that are larger or smaller than the Lindblad result, and that are not centered on the same value of ΔE .

Figure 6d shows the transfer rates for the hightemperature parameter set. For the Lindblad simulation, the transfer rate initially increased as the energy gap increased but then decreased after the energy gap was larger than the reorganization energy of 20 $\hbar\omega$, showing Marcus inverted region behavior. Repeated interaction simulations with larger interaction lengths showed this same general behavior but had numerous small oscillations, rather than a single broad peak. As the repeated interaction length decreased, the oscillations in the transfer rate disappeared. For $\tau = 0.01(2\pi/\omega)$, the transfer rates were slightly larger than the Lindblad results, but with $\tau = 0.01(2\pi/\omega)$, the results converged to the Lindblad rates, meaning that ten times as small of a step was needed compared to the low-temperature DA parameters.

By evolving an easy-to-prepare state with a repeated interaction model that did not contain the electronic coupling, we prepared states that had high fidelity with the exact initial state (Equation 13) for all parameter regimes for the DA model and the DBA system. As shown in Figure 7, the state preparation procedure generated states with above 99% fidelity compared to the exact initial states within $t = 400(2\pi/\omega)$ for all the parameter sets. Note that because the exact initial state does not depend on the electronic coupling or the damping rate, the three low-temperature $(k_{\rm B}T=1\hbar\omega)$ parameter sets have the same initial state. The fidelity for the high-temperature parameters rose quickly and then plateaued, while for the weakly coupled and DBA systems, it increased slowly. Even though the parameter sets led to different behaviors in how the fidelity increases, the state preparation procedure was still capable of generating high-fidelity states after a short time evolution.

Factoring the repeated interaction unitary using a 2ndorder Trotter formula (Equation 16) led to small per-

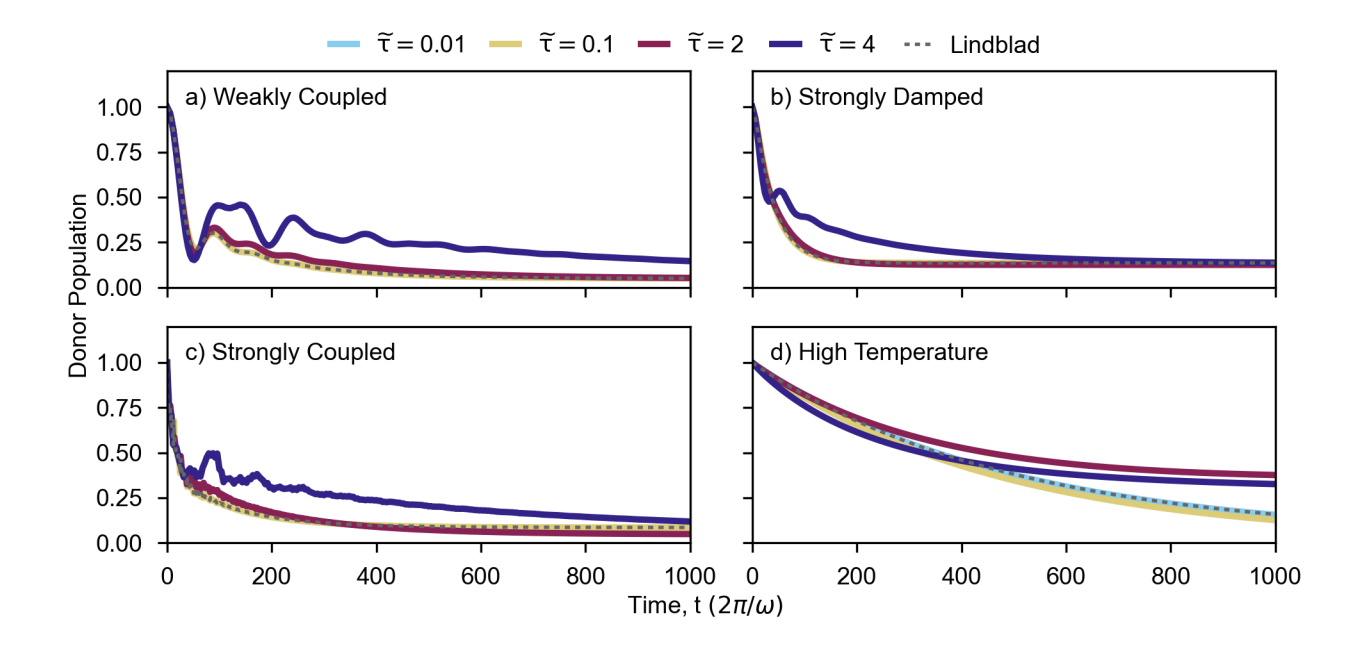


FIG. 4. Repeated Interaction Simulations. Donor populations from repeated interaction simulations of the (a) weakly coupled, (b) strongly damped, (c) strongly coupled, and (d) high-temperature parameter sets as a function of time, t. Colors show the donor populations for different values of the repeated interaction length, with $\tilde{\tau} = \tau \omega/(2\pi)$. Dashed lines show reference populations from Lindblad simulations. The energy separations ΔE were set to: $3\hbar\omega$ for weakly coupled, $2\hbar\omega$ for strongly damped, $4.4\hbar\omega$ for strongly coupled, and $20\hbar\omega$ for high-temperature parameter sets. The agreement between the repeated interaction and Lindblad simulations across all parameter sets demonstrates the reliability of the repeated interaction model in capturing electron transfer dynamics.

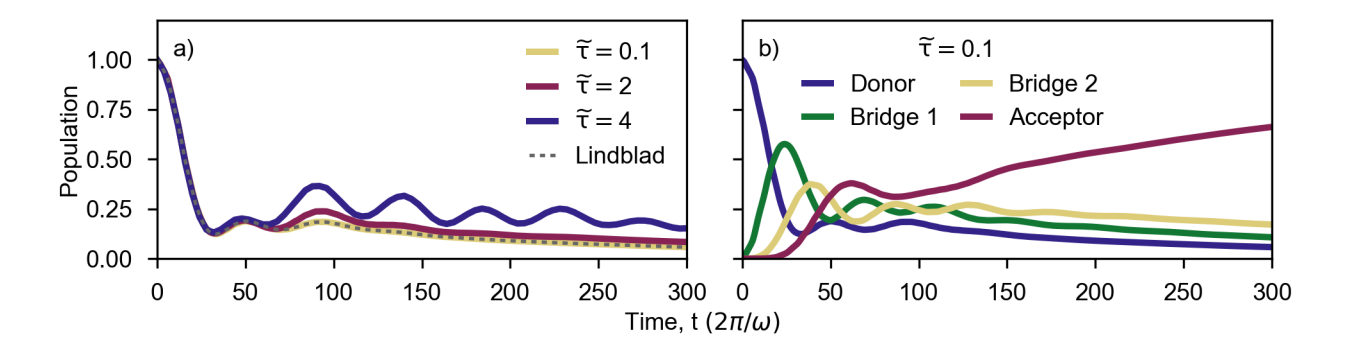


FIG. 5. **Donor-Bridge-Acceptor Populations.** Colors in (a) show the donor population for different values of the repeated interaction length, with $\tilde{\tau} = \tau \omega/(2\pi)$ for the donor-bridge-acceptor parameter set. The dashed line shows the reference donor population from a Lindblad simulation. (b) Populations of the donor, bridges, and acceptor from repeated interaction simulations with $\tau = 0.1(2\pi/\omega)$. The sequential population transfer from the donor to the acceptor via the bridge sites reflects a stepwise hopping mechanism with coherent oscillations. These results illustrate how the repeated interaction model captures intermediate bridge site dynamics, highlighting its ability to resolve multi-step electron transfer processes, as well as investigating how the algorithm scales when the system size is increased.

cent errors in the calculated transfer rates for all of the parameter sets tested for the DA model system. For a single Trotter step per repeated interaction (n=1), the percent error in the transfer rate was less than 4% for all of the parameter regimes, as shown in Figure 8, where the energy gap, ΔE , was chosen to give the largest transfer rate. The percent error was the smallest for the high-temperature parameters, likely due to the

shorter interaction length needed to converge to Lindblad dynamics. Because of the small percent error and the increased computational demand for simulations of the high-temperature parameters, we did not go beyond 25 Trotter steps per repeated interaction. Interestingly, for all the parameter sets, the percent error in the transfer rate did not monotonically decrease as the number of Trotter steps increased. For the low-temperature parameters

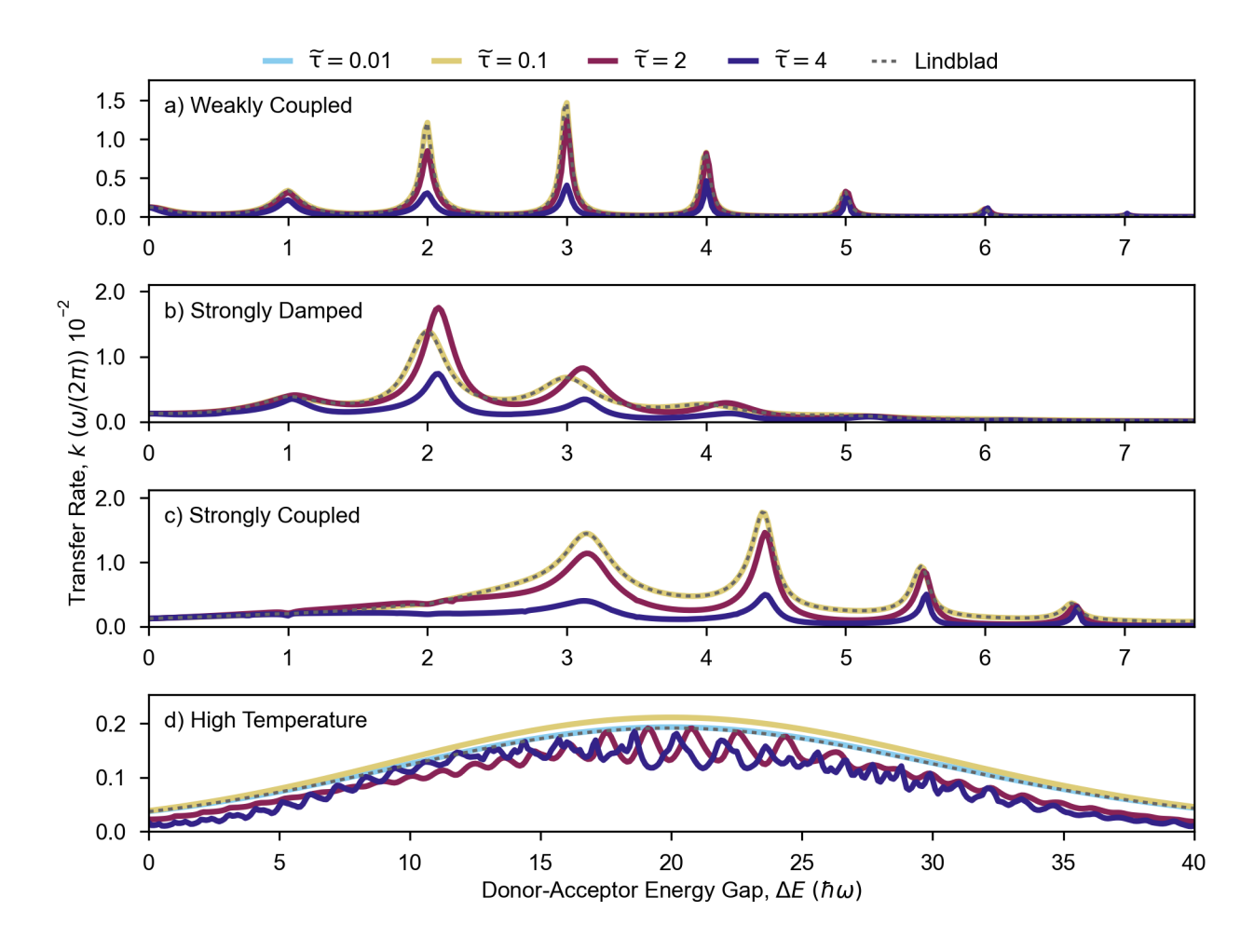


FIG. 6. Electron Transfer Rates. Transfer rates, k, from repeated interaction simulations of the weakly coupled (a), strongly damped (b), strongly coupled (c), and high-temperature (d) parameters as a function of donor-acceptor energy separation, ΔE . Colors show the transfer rates for different values of the repeated interaction length, with $\tilde{\tau} = \tau \omega/(2\pi)$. Dashed lines show reference transfer rates from Lindblad simulations. The consistency between the repeated interaction and Lindblad simulations across all parameter sets validates the accuracy of the repeated interaction model in capturing electron transfer dynamics.

eters, the percent error had a local minimum between n=2 and n=5, while for the high temperature, n=1 was a local minimum. Above 30 Trotter steps per repeated interaction, the percent error steadily decreased for the low-temperature sets.

V. DISCUSSION

Our numerical simulations of the repeated interaction model successfully generated non-Markovian ET dynamics without needing prohibitively small repeated interaction length for any of the parameter regimes tested. This result shows promise for applying quantum algorithms based on repeated interaction models to open chemical systems. State preparation was straightforward using the repeated interaction method, where input states with over 99% fidelity were generated over a short time evolution. The practical utility of this method was further

confirmed by examining how the error introduced by the Trotter formula scales with the number of Trotter steps. For the systems studied, we found that a single Trotter step per repeated interaction produced an acceptable error of less than 4%. While the number of Trotter steps could be optimized for these types of systems, we expect adequately low Trotter errors to be found in just a few Trotter steps per repeated interaction. Seeing as the dynamics are already discretized into small steps for the repeated interaction method, it is unsurprising that a single Trotter step per repeated interaction was sufficient. Taken together, this seems like a promising avenue for simulating non-unitary dynamics for chemistry on a unitary quantum computer.

To evaluate the performance of the quantum algorithm, we compared the required number of repeated interactions to the analytical upper bound given by Pocrnic et al. 45

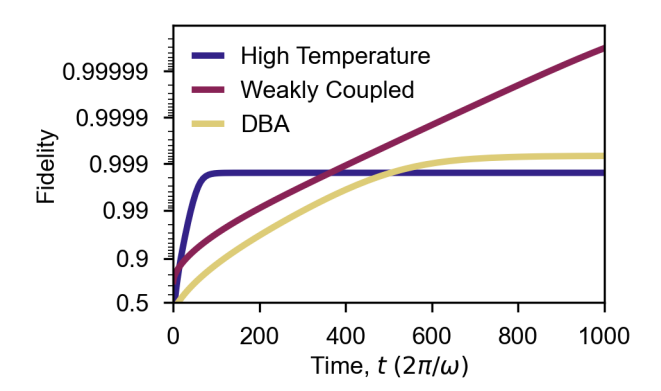


FIG. 7. Fidelity of Prepared Initial State. Fidelity between the exact initial state and the state following the state preparation procedure as a function of simulation time for the weakly coupled, high-temperature, and donor-bridge-acceptor (DBA) parameter sets. The state preparation begins with the electronic system in the donor state and the oscillator in the ground state and then evolves in time with a repeated interaction model that does not contain electronic coupling. The three parameter sets with $k_{\rm B}T=1\hbar\omega$ have the same initial state, so we only show the weakly coupled set. The fidelity quickly increases across all parameter sets, confirming that the state preparation scheme reliably initializes the system for repeated interaction simulations.

$$s \in O\left(\frac{t^2}{\epsilon} \left(\|\mathcal{L}\|_{1 \to 1}^2 + \max\{\|H_{\text{ET}}\|, \|H_{\text{int}}\|\}^4 \right) \right), \quad (17)$$

where s is the number of repeated interactions needed to converge to Lindblad dynamics, t is the total time of the simulation, and ϵ is the error. $\|\mathcal{L}\|_{1\to 1}$ is the induced Schatten $1\to 1$ norm of the Lindbladian superoperator (Equation 3), defined as $\|\mathcal{L}\|_{1\to 1} = \max_A \|\mathcal{L}(A)\|_1$, where $\|A\|_1 = 1$. This induced superoperator norm is difficult to calculate exactly because it requires optimizing over all possible matrices with unit norm. To estimate this norm we perform Monte Carlo sampling over Hermitian matrices, with ΔE set to the highest value used for each parameter set. Our estimates are strictly less than the actual induced norm because there could be non-Hermitian matrices that give a larger value for $\|\mathcal{L}(A)\|_1$, meaning that we might underestimate the upper bound for the number of repeated interactions.

Table II presents the analytical worst-case upper bound and our simulation results for the required number of repeated interactions to converge to the Lindblad dynamics for the DA models relative to the weakly coupled parameter set. While the simulation results for the strongly damped and strongly coupled parameter sets align with the analytical bound, the high-temperature set has much better scaling. Despite the upper bound for the high-temperature system being over 1300 times larger than for the weakly coupled system, our simulations only required 10 times more repeated interactions,

illustrating the robustness of the method under challenging conditions for chemically relevant parameter regimes. The observed scaling behavior underscores a critical insight: while the analytical worst-case bounds for operator norms predict significant computational challenges for certain systems (notably, the high-temperature regime), our empirical results demonstrate far more efficient scaling in practice. This discrepancy highlights the value of simulation-driven evaluation, which captures algorithmic performance under realistic conditions better than relying solely on theoretical bounds.

TABLE II. Required Number of Repeated Interactions Relative to Weakly Coupled Parameter Set. The analytical upper bounds come from Equation 17.

Parameter set	Analytical	Observed
Strongly damped	1.0032	1
Strongly coupled	1.0192	1
High temperature	1361.6	10

The SVD-based approach, as demonstrated in simulations of the FMO complex, 43,44 effectively maps non-unitary dynamics onto quantum circuits, making it well-suited for NISQ hardware. However, its dependence on classical diagonalization introduces a scaling bottleneck, particularly for larger systems or those with strong correlations and memory effects. While quantum singular value transformation has been proposed as a potential way to bypass this classical step, 20 the necessity of diagonalization remains a fundamental constraint when dealing with large systems.

By contrast, the repeated interaction model provides a direct encoding of the system-environment interaction into the quantum simulation, without the need for matrix decomposition. This makes it a promising alternative, especially for scenarios where environmental effects are significant and non-trivial to approximate classically. Given that we observe convergence to Lindblad dynamics with relatively few iterations, repeated interaction avoids the computational overhead that might otherwise be a concern.

Ultimately, the suitability of each method depends on the problem at hand. For relatively simple, well-characterized dynamics like those of the FMO complex, SVD remains a powerful tool. However, for more complex open quantum systems where system-environment interactions play a crucial role, repeated interaction, and other variational approaches may offer a more scalable and physically transparent framework. The trade-offs between classical preprocessing, circuit depth, and accuracy should be carefully considered when selecting the most appropriate algorithm.

Recent analog quantum simulations of ET reactions on real quantum hardware have demonstrated the potential of near-term quantum devices for studying open quantum systems. Trapped-ion and superconducting qubit platforms have been used to model dissipative and coherent dynamics, providing experimental validation of theoreti-

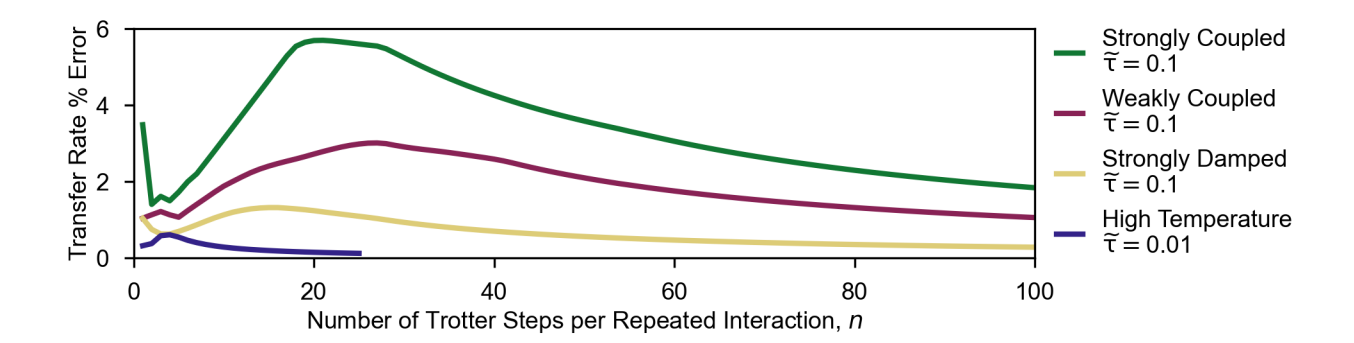


FIG. 8. Error from Using Trotter Formula. Percent error in the transfer rates as a function of the number of Trotter steps per repeated interaction n from 2nd-order Trotter simulations of repeated interaction schemes relative to exact simulations with no Trotterization. The repeated interaction length, labeled with $\tilde{\tau} = \tau \omega/(2\pi)$, is ten times shorter for the high-temperature case. The energy separations ΔE were set to the largest peaks: $4.4\hbar\omega$ for strongly coupled, $3\hbar\omega$ for weakly coupled, $2\hbar\omega$ for strongly damped, and $20\hbar\omega$ for high-temperature parameter sets. These results demonstrate that Trotterization error decreases with increasing Trotter steps, with the strongest errors observed in strongly coupled systems which has faster dynamics. For high-temperature systems, the same would be expected, but the finer time discretization required for this parameter set alleviates the need for more Trotter steps per repeated interaction.

cal frameworks.¹⁰ However, despite these advances, current analog simulations remain restricted to parameter regimes set by the hardware, preventing the exploration of classical reaction limits. This highlights a fundamental limitation of analog approaches, as they cannot easily access the full range of system-bath interactions predicted in theoretical models.

In the near term, different quantum approaches will likely be suited to different aspects of open quantum system simulations. Digital algorithms such as repeated interactions, quantum singular value transformations, and variational master equation solvers provide a flexible framework that can be adapted to various systemenvironment interactions, while analog quantum simulations may offer advantages for specific systems if the experimental system naturally mimics the desired interaction, has strong intersystem correlations compared to system-environment correlations or has a structured connectivity which fits with a specific device. As faulttolerant quantum hardware becomes more accessible, the scalability and programmability of digital methods will make them increasingly dominant, particularly for simulating complex chemical dynamics with strong systembath correlation and highly structured environments. Key developments to watch include advances in quantum error correction, the implementation of noise-resilient gates, and improved encodings of open system dynamics onto logical qubits. Ultimately, the choice of method will depend on the nature of the system under study, with digital and analog approaches serving complementary roles in different problem regimes.

VI. CONCLUSION

We have shown that quantum algorithms based on a repeated interaction model can reproduce non-Markovian ET dynamics across realistic chemical parameter regimes. Additionally, we have shown that the algorithm scales better than expected in terms of the number of repeated interactions needed as the temperature increases. When fault-tolerant quantum hardware becomes available, we expect this algorithm to be useful for modeling real systems, where more complexity could be incorporated by adding structured baths, multidimensional reaction coordinates, or more intricate coupling schemes. Our findings suggest that repeated interaction models provide an efficient and scalable approach to simulating open quantum systems, particularly for parameter regimes relevant to ET. In future work, it would be valuable to benchmark this approach against both classical and quantum algorithms for larger and more complex molecular systems with applications such as enzymatic catalysis or molecular electronics. A key open question is whether scalable, repeated interaction algorithms can be designed to reproduce non-Markovian dynamics of chemical systems without needing to use the reaction coordinate supersystem approach. As quantum hardware advances, we hope quantum simulations based on repeated interactions will help chemists elucidate real-world chemical dynamics at the quantum level.

ACKNOWLEDGMENTS

We thank Prof. Dvira Segal and Matthew Pocrnic for fruitful discussions regarding the repeated interaction model. This work is supported by the Novo Nordisk Foundation, grant number NNF22SA0081175,

NNF Quantum Computing Programme. M.S.T. acknowledges support from the Novo Nordisk Foundation (Challenge project "Solid-Q").

CODE AVAILABILITY

The code used for these simulations is available on GitHub at https://github.com/mteynor/ri4et.

REFERENCES

- ¹Y. Cao, J. Romero, J. P. Olson, M. Degroote, P. D. Johnson, M. Kieferová, I. D. Kivlichan, T. Menke, B. Peropadre, N. P. D. Sawaya, S. Sim, L. Veis, and A. Aspuru-Guzik, Chem. Rev. 119, 10856 (2019), publisher: American Chemical Society.
- ²A. J. Daley, I. Bloch, C. Kokail, S. Flannigan, N. Pearson, M. Troyer, and P. Zoller, Nature 607, 667 (2022), publisher: Nature Publishing Group.
- ³C.-F. Li, G.-C. Guo, and J. Piilo, EPL **127**, 50001 (2019), publisher: EDP Sciences, IOP Publishing and Società Italiana di Fisica.
- ⁴L. Li, M. J. W. Hall, and H. M. Wiseman, Physics Reports Concepts of quantum non-Markovianity: A hierarchy, **759**, 1 (2018).
- ⁵M. A. Nielsen and I. L. Chuang, Quantum computation and quantum information, 10th ed. (Cambridge university press, Cambridge, 2010).
- ⁶S. Mostame, P. Rebentrost, A. Eisfeld, A. J. Kerman, D. I. Tsomokos, and A. Aspuru-Guzik, New Journal of Physics 14, 105013 (2012), arXiv:1106.1683 [quant-ph].
- ⁷L. García-Álvarez, U. Las Heras, A. Mezzacapo, M. Sanz, E. Solano, and L. Lamata, Sci Rep 6, 27836 (2016), publisher: Nature Publishing Group.
- ⁸A. Lemmer, C. Cormick, D. Tamascelli, T. Schaetz, S. F. Huelga, and M. B. Plenio, New J. Phys. **20**, 073002 (2018), publisher: IOP Publishing.
- ⁹R. J. MacDonell, C. E. Dickerson, C. J. T. Birch, A. Kumar, C. L. Edmunds, M. J. Biercuk, C. Hempel, and I. Kassal, Chem. Sci. 12, 9794 (2021), publisher: The Royal Society of Chemistry.
- ¹⁰F. Schlawin, M. Gessner, A. Buchleitner, T. Schätz, and S. S. Skourtis, PRX Quantum 2, 010314 (2021), publisher: American Physical Society.
- ¹¹C. W. Kim, J. M. Nichol, A. N. Jordan, and I. Franco, PRX Quantum 3, 040308 (2022), publisher: American Physical Society.
- ¹²C. Sparrow, E. Martín-López, N. Maraviglia, A. Neville, C. Harrold, J. Carolan, Y. N. Joglekar, T. Hashimoto, N. Matsuda, J. L. O'Brien, D. P. Tew, and A. Laing, Nature 557, 660 (2018), publisher: Nature Publishing Group.
- ¹³V. So, M. Duraisamy Suganthi, A. Menon, M. Zhu, R. Zhuravel, H. Pu, P. G. Wolynes, J. N. Onuchic, and G. Pagano, Science Advances 10, eads8011 (2024), publisher: American Association for the Advancement of Science.
- ¹⁴K. Sun, M. Kang, H. Nuomin, G. Schwartz, D. N. Beratan, K. R. Brown, and J. Kim, "Quantum Simulation of Spin-Boson Models with Structured Bath," (2024), arXiv:2405.14624 [quant-ph].
- ¹⁵T. Navickas, R. J. MacDonell, C. H. Valahu, V. C. Olaya-Agudelo, F. Scuccimarra, M. J. Millican, V. G. Matsos, H. L. Nourse, A. D. Rao, M. J. Biercuk, C. Hempel, I. Kassal, and T. R. Tan, "Experimental Quantum Simulation of Chemical Dynamics," (2024), arXiv:2409.04044 [quant-ph].
- ¹⁶H. Tang, X.-W. Shang, Z.-Y. Shi, T.-S. He, Z. Feng, T.-Y. Wang, R. Shi, H.-M. Wang, X. Tan, X.-Y. Xu, Y. Wang, J. Gao, M. S. Kim, and X.-M. Jin, npj Quantum Inf **10**, 29 (2024).

- ¹⁷B.-X. Wang, M.-J. Tao, Q. Ai, T. Xin, N. Lambert, D. Ruan, Y.-C. Cheng, F. Nori, F.-G. Deng, and G.-L. Long, npj Quantum Inf 4, 1 (2018), publisher: Nature Publishing Group.
- ¹⁸Z. Hu, R. Xia, and S. Kais, Scientific Reports 10, 3301 (2020), publisher: Nature Publishing Group.
- ¹⁹A. W. Schlimgen, K. Head-Marsden, L. M. Sager, P. Narang, and D. A. Mazziotti, Physical Review Letters **127**, 270503 (2021), publisher: American Physical Society.
- ²⁰N. Suri, J. Barreto, S. Hadfield, N. Wiebe, F. Wudarski, and J. Marshall, Quantum 7, 1002 (2023), publisher: Verein zur Förderung des Open Access Publizierens in den Quantenwissenschaften.
- ²¹A. W. Schlimgen, K. Head-Marsden, L. M. Sager-Smith, P. Narang, and D. A. Mazziotti, Physical Review A **106**, 022414 (2022), publisher: American Physical Society.
- ²²A. Gaikwad, Arvind, and K. Dorai, Physical Review A 106, 022424 (2022), publisher: American Physical Society.
- ²³Z. Ding, X. Li, and L. Lin, PRX Quantum 5, 020332 (2024), publisher: American Physical Society.
- ²⁴T. Basile and C. Pineda, PLOS ONE 19, e0297210 (2024), publisher: Public Library of Science.
- ²⁵ J. Xuereb, S. Campbell, J. Goold, and A. Xuereb, Physical Review A 107, 042222 (2023), publisher: American Physical Society.
- ²⁶H. Kamakari, S.-N. Sun, M. Motta, and A. J. Minnich, PRX Quantum 3, 010320 (2022), publisher: American Physical Society.
- ²⁷S. Endo, J. Sun, Y. Li, S. C. Benjamin, and X. Yuan, Physical Review Letters **125**, 010501 (2020), publisher: American Physical Society.
- ²⁸S. Shivpuje, M. Sajjan, Y. Wang, Z. Hu, and S. Kais, Advanced Quantum Technologies n/a, 2400088 (2024), _eprint: https://onlinelibrary.wiley.com/doi/pdf/10.1002/qute.202400088.
- ²⁹T. M. Watad and N. H. Lindner, Quantum Science and Technology 9, 025015 (2024), publisher: IOP Publishing.
- ³⁰ J. Luo, K. Lin, and X. Gao, The Journal of Physical Chemistry Letters 15, 3516 (2024), publisher: American Chemical Society.
- ³¹M. Mahdian and H. D. Yeganeh, Journal of Physics A: Mathematical and Theoretical 53, 415301 (2020), publisher: IOP Publishing.
- ³²H.-Y. Liu, T.-P. Sun, Y.-C. Wu, and G.-P. Guo, Chinese Physics Letters 38, 080301 (2021), publisher: Chinese Physical Society and IOP Publishing Ltd.
- ³³ J. W. Z. Lau, K. H. Lim, K. Bharti, L.-C. Kwek, and S. Vinjanampathy, Physical Review Letters 130, 240601 (2023), publisher: American Physical Society.
- ³⁴J. Joo and T. P. Spiller, New Journal of Physics **25**, 083041 (2023), publisher: IOP Publishing.
- ³⁵N. Suri, F. C. Binder, B. Muralidharan, and S. Vinjanampathy, The European Physical Journal Special Topics 227, 203 (2018).
- ³⁶S. Santos, X. Song, and V. Savona, "Low-Rank Variational Quantum Algorithm for the Dynamics of Open Quantum Systems," (2025), eprint: 2403.05908.
- ³⁷C. K. Lee, P. Patil, S. Zhang, and C. Y. Hsieh, Physical Review Research 3, 023095 (2021), publisher: American Physical Society.
- ³⁸P. J. Ollitrault, S. Jandura, A. Miessen, I. Burghardt, R. Martinazzo, F. Tacchino, and I. Tavernelli, Quantum 7, 1139 (2023), publisher: Verein zur Förderung des Open Access Publizierens in den Quantenwissenschaften.
- ³⁹L. Gravina and V. Savona, Physical Review Research 6, 023072 (2024), publisher: American Physical Society.
- ⁴⁰D. S. Schlegel, F. Minganti, and V. Savona, "Coherent-State Ladder Time-Dependent Variational Principle for Open Quantum Systems," (2023), arXiv:2306.13708 [quant-ph].
- ⁴¹H. Zhou, R. Mao, and X. Sun, "Hybrid algorithm simulating non-equilibrium steady states of an open quantum system," (2023), arXiv:2309.06665 [quant-ph].
- ⁴²N. Lyu, E. Mulvihill, M. B. Soley, E. Geva, and V. S. Batista, Journal of Chemical Theory and Computation 19, 1111 (2023),

- publisher: American Chemical Society.
- ⁴³Z. Hu, K. Head-Marsden, D. A. Mazziotti, P. Narang, and S. Kais, Quantum 6, 726 (2022), publisher: Verein zur Förderung des Open Access Publizierens in den Quantenwissenschaften.
- ⁴⁴X. Dan, E. Geva, and V. S. Batista, J. Chem. Theory Comput. (2025), 10.1021/acs.jctc.4c01565, publisher: American Chemical Society.
- ⁴⁵M. Pocrnic, D. Segal, and N. Wiebe, "Quantum Simulation of Lindbladian Dynamics via Repeated Interactions," (2024), arXiv:2312.05371 [quant-ph].
- ⁴⁶F. Gallina, M. Bruschi, and B. Fresch, New J. Phys. **24**, 023039 (2022), publisher: IOP Publishing.
- ⁴⁷F. Gallina, M. Bruschi, R. Cacciari, and B. Fresch, Journal of Chemical Theory and Computation 20, 10588 (2024), publisher: American Chemical Society.
- ⁴⁸F. Ciccarello, S. Lorenzo, V. Giovannetti, and G. M. Palma, Physics Reports Quantum collision models: Open system dynamics from repeated interactions, 954, 1 (2022).
- ⁴⁹A. Nitzan, Chemical dynamics in condensed phases: relaxation, transfer and reactions in condensed molecular systems, Oxford Graduate Texts (Oxford University Press, Oxford, 2006).
- ⁵⁰O. K. Volkhard May, Charge and Energy Transfer Dynamics in Molecular Systems, 3rd ed. (Wiley, Newark, 2011).
- ⁵¹N. Anto-Sztrikacs and D. Segal, Phys. Rev. A **104**, 052617 (2021), publisher: American Physical Society.
- ⁵²H. Breuer and F. Petruccione, The Theory of Open Quantum Systems (Oxford University Press, 2002).
- ⁵³L. Zhang, F. Fassioli, B. Fu, Z.-S. She, and G. D. Scholes, ACS Phys. Chem Au 3, 107 (2023), publisher: American Chemical Society.
- ⁵⁴A. Rivas, S. F. Huelga, and M. B. Plenio, Phys. Rev. Lett. **105**, 050403 (2010), publisher: American Physical Society.
- ⁵⁵M. Suzuki, Physics Letters A **146**, 319 (1990).

Supplementary Material:

A Digital Quantum Algorithm for Non-Markovian Electron Transfer Dynamics Using Repeated Interactions

Lea K. Northcote, ^{1, a)} Matthew S. Teynor, ^{1, 2, a)} and Gemma C. Solomon^{1, 2, b)}

(Dated: 25 February 2025)

I. HARMONIC OSCILLATOR TRUNCATION

For numerical simulations of harmonic oscillators, we have to truncate the infinite-dimensional Hilbert space to a finite number of energy levels. This truncation is also required for digital quantum simulations, where the oscillator is encoded into a qubit register. With binary encoding, n qubits can encode 2^n energy levels. To systematically choose the number of qubits required to encode the harmonic oscillator in the electron transfer (ET) model systems, we evaluated the initial position as well as the transfer rate error from Lindblad simulations for different numbers of qubits. Figure S1 shows the position of the truncated harmonic oscillator for the initial states of the weakly coupled (which has the same initial state as the strongly coupled and strongly damped parameters) and high-temperature donor-acceptor systems, compared to the exact initial position $-\sqrt{\lambda/(\hbar\omega)}/2$. The weakly coupled case has the correct initial position when there are at least four qubits (16 energy levels). The high-temperature system requires five qubits (32 energy levels) before it has the correct initial position. Figure S2 and Figure S3 show the transfer rates for three, four, and five qubits, as well as the percent error in the transfer rate relative to using six qubits. We achieve a maximum error of less than 2% in the transfer rate with four qubits for the weakly coupled and five qubits for the high-temperature parameter sets.

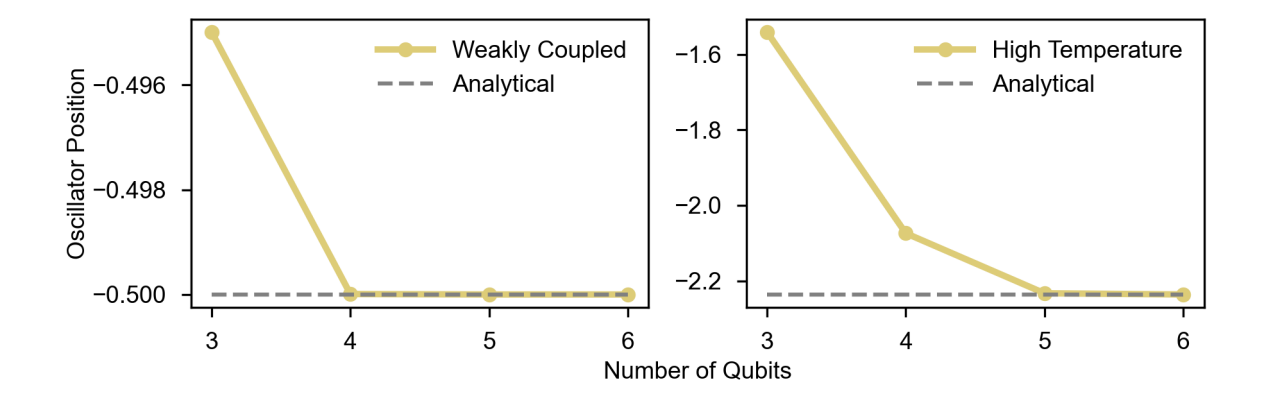


FIG. S1. Expectation Value of Position Operator for the Harmonic Oscillator Across Regimes. The first oscillator position in the simulations was evaluated for $\Delta E = 3\hbar\omega$ for the weakly coupled parameter set and $\Delta E = 20\hbar\omega$ for the high-temperature parameter set. The analytical solution is shown with a dashed line. The weakly coupled parameter set converges with four qubits corresponding to 16 energy levels. The high-temperature parameter set requires five qubits corresponding to 32 energy levels to represent the harmonic oscillator position sufficiently.

¹⁾NNF Quantum Computing Programme, Niels Bohr Institute, University of Copenhagen, DK-2100 Copenhagen Ø, Denmark

²⁾ Nano-Science Center and Department of Chemistry, University of Copenhagen, DK-2100 Copenhagen Ø, Denmark

a) Contributed equally

b) Email: gsolomon@chem.ku.dk

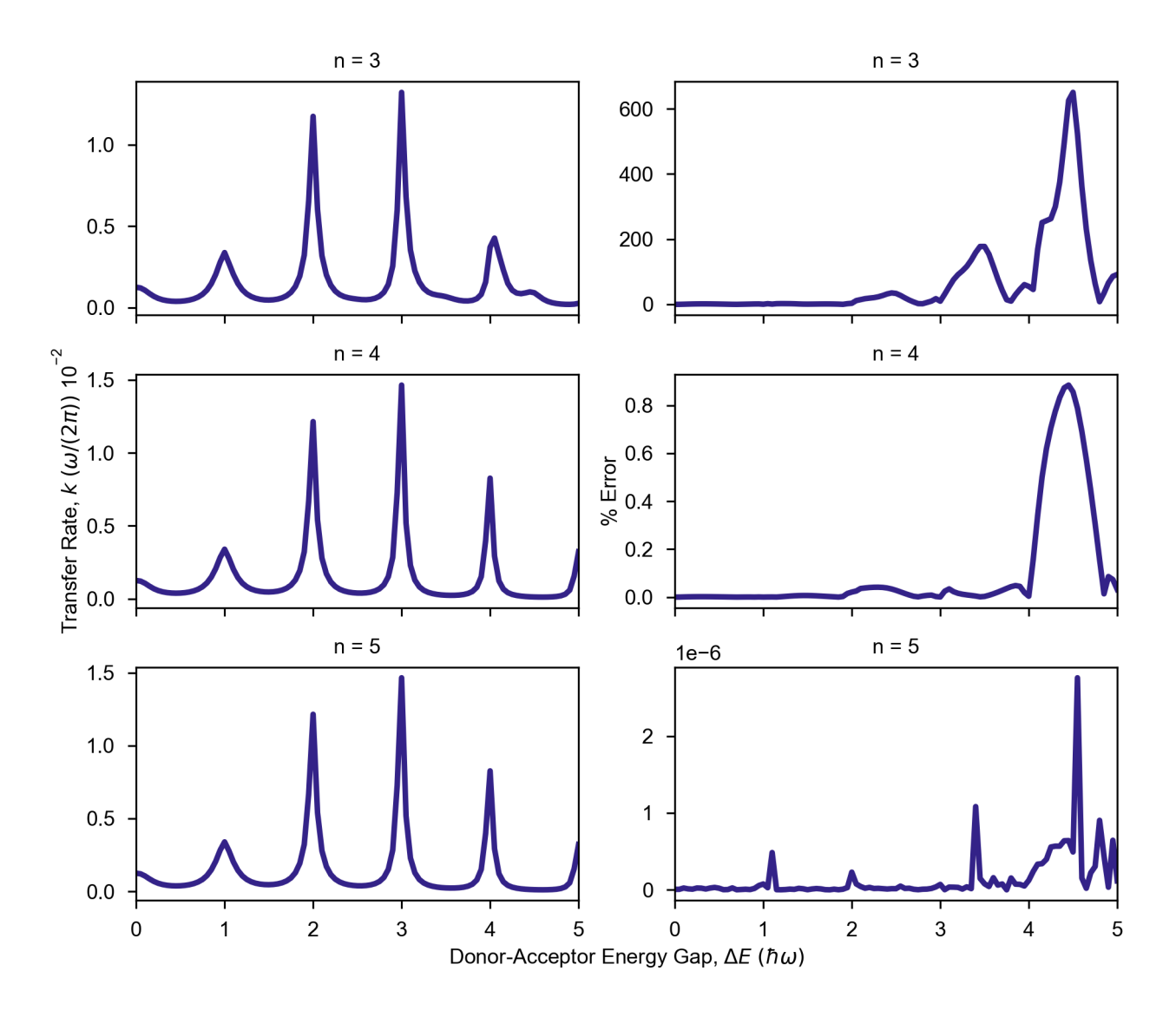


FIG. S2. Harmonic Oscillator Truncation for the Weakly Coupled Parameter Set. For n = 3 to 5 qubits, the electron transfer rates and the percentage error relative to n = 6 qubits are shown as a function of the donor-acceptor energy gap.

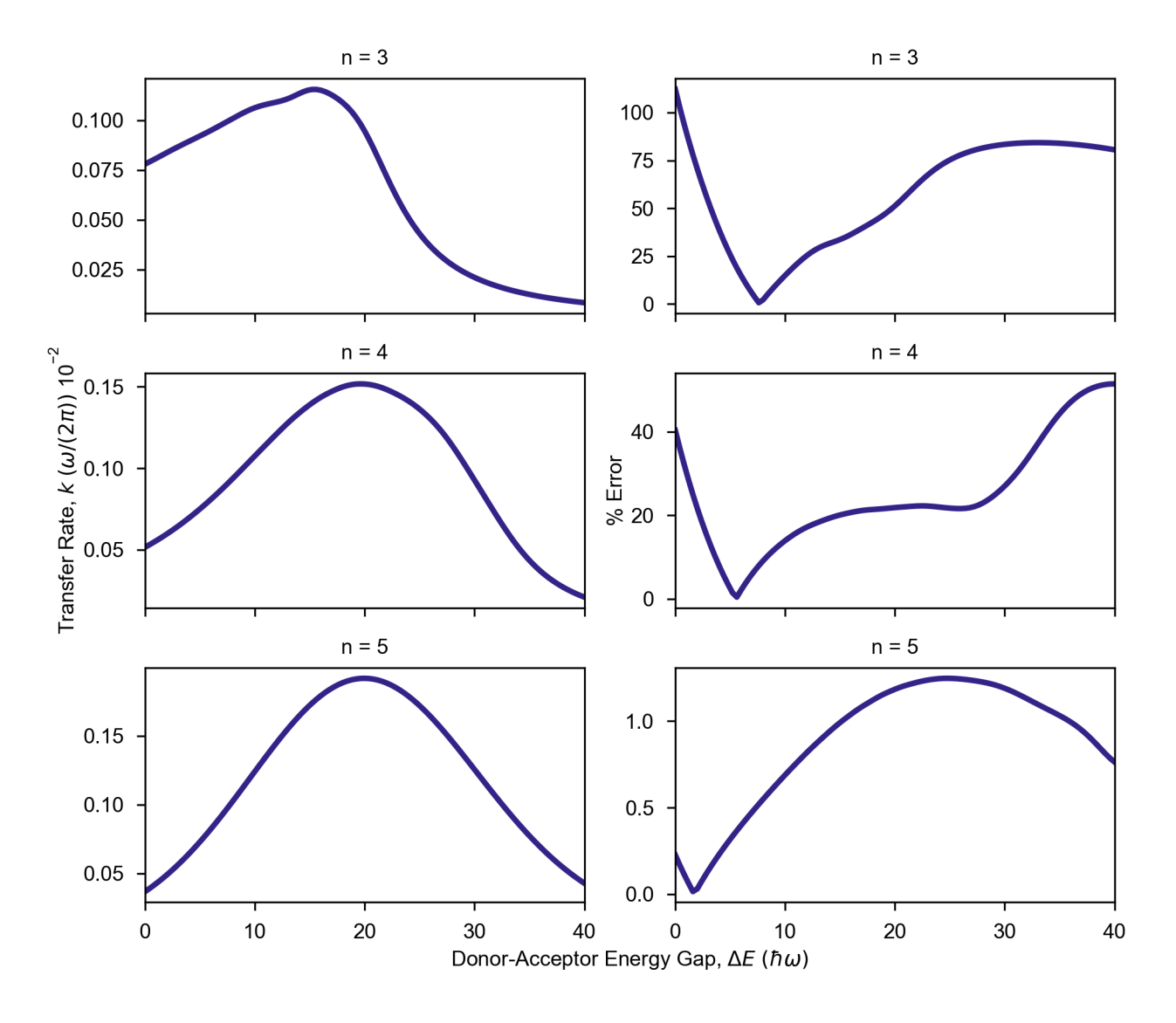


FIG. S3. Harmonic Oscillator Truncation for the High-Temperature Parameter Set. For n=3 to 5 qubits, the electron transfer rates and the percentage error relative to n=6 qubits are shown as a function of the donor-acceptor energy gap.

II. PRESERVATION OF NON-MARKOVIAN DYNAMICS IN THE REPEATED INTERACTION MODEL

We confirmed that our parameter regimes displayed non-Markovian dynamics by measuring the degree of non-Markovianity using the Rivas, Huelga, Plenio (RHP) measure. This involves starting a simulation with the electronic system maximally entangled with a non-interacting ancilla (which is separate from the ancilla used for the repeated interactions). We then calculate the concurrence, a measure of entanglement, between the electronic system and the non-interacting ancilla throughout the simulation. With Markovian dynamics, the entanglement will monotonically decrease throughout the simulation, because information can not flow back from the reaction coordinate into the electronic system. The RHP measure is found by integrating over the concurrence as

$$\mathcal{I}^{(E)} = \int_{t_0}^{t_{\text{max}}} \left| \frac{\mathrm{d}\mathcal{E}[\rho_{\text{SA}}(t)]}{\mathrm{d}t} \right| \mathrm{d}t - \Delta\mathcal{E}, \tag{1}$$

with

$$\Delta \mathcal{E} = \mathcal{E}[\rho_{SA}(t_0)] - \mathcal{E}[\rho_{SA}(t_{\text{max}})] \tag{2}$$

where $\mathcal{E}[\rho_{\mathrm{SA}}(t)]$ is the concurrence between the electronic system and the non-interacting ancilla at time t. If the entanglement measure increases at any point, leading to an RHP measure greater than zero, the dynamics are non-Markovian. For the four donor-acceptor parameter sets, we plot the RHP measure as a function of the donor-acceptor energy gap from Lindblad simulations in Figure S4. This shows that the low-temperature parameter sets all have non-Markovian dynamics. To ensure that the repeated interaction model does not change the RHP measure, we plot the concurrence in Figure S5 as a function of time for the weakly coupled parameter set with $\Delta E = 3\hbar\omega$, with the Lindblad simulation results as a reference. We see the same increases in entanglement for the repeated interaction model, confirming that as the repeated interaction model converges to the Lindblad result, the backflow of information from the reaction coordinate to the electronic system is preserved.

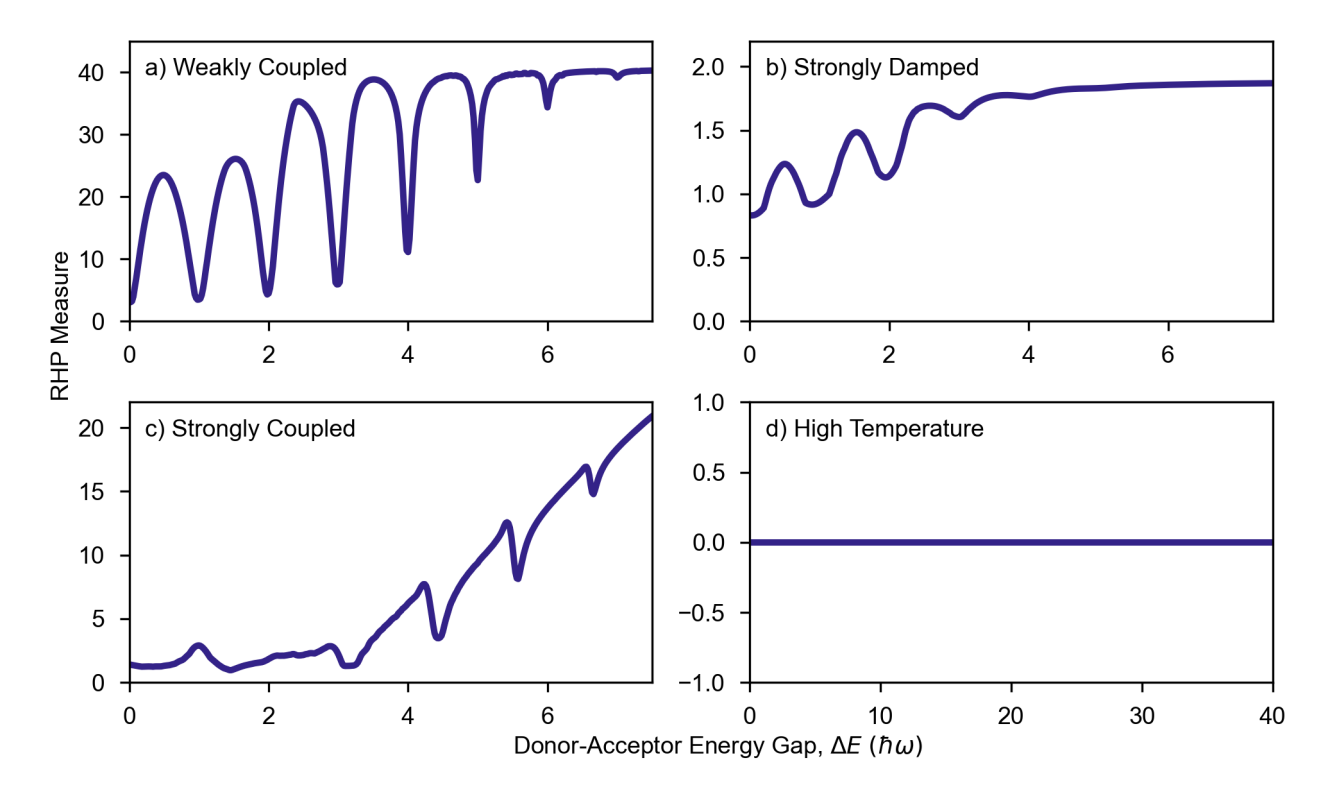


FIG. S4. Rivas, Huelga, Plenio Measures for the Donor-Acceptor Parameter Sets. The measure is non-zero, indicating non-Markovian dynamics, for all values of the donor-acceptor energy gap for the low-temperature parameter sets.

¹A. Rivas, S. F. Huelga, and M. B. Plenio, Phys. Rev. Lett. **105**, 050403 (2010), publisher: American Physical Society.

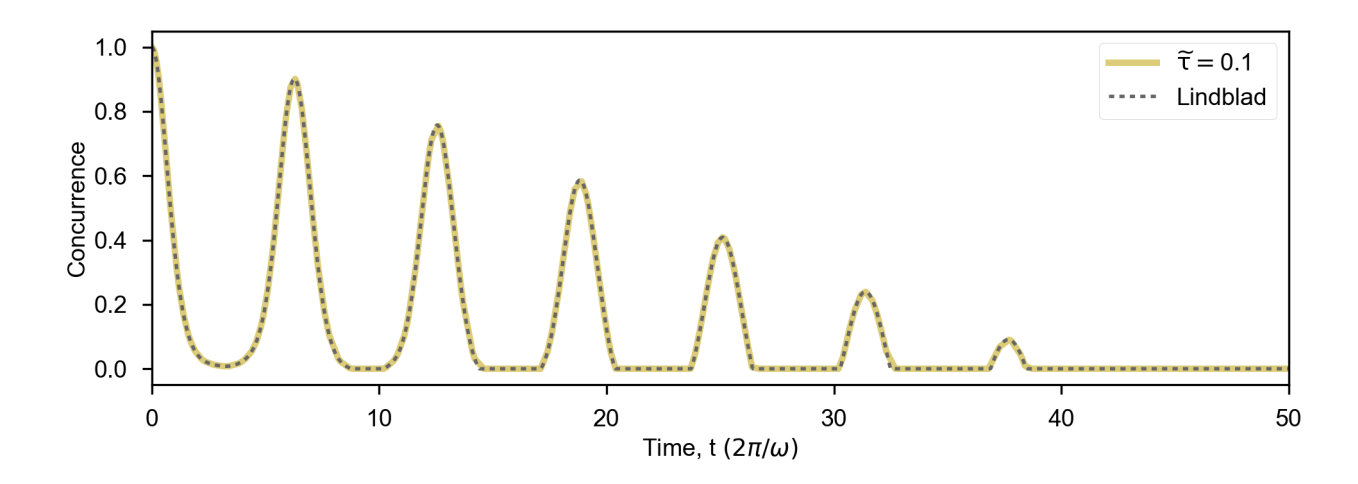


FIG. S5. Concurrence Used in the Rivas, Huelga, Plenio Measure from a Repeated Interaction Simulation. For the weakly coupled parameter set with $\Delta E=3\hbar\omega$, the entanglement between the electron and a non-interacting ancilla (started in a maximally entangled state) is shown as a function of time. The concurrence does not monotonically decrease, showing non-Markovian dynamics. The repeated interaction simulation with $\tau=0.1(2\pi/\omega)$ matches the Lindblad simulation result.